The Astrophysical Journal, 767:81 (8pp), 2013 April 10 doi:10.1088/0004-637X/767/1/81

HYDROGEN CHLORIDE IN DIFFUSE INTERSTELLAR CLOUDS ALONG THE LINE OF SIGHT TO W31C (G10.6-0.4)

R. R. Monje[1], D. C. Lis[1], E. Roueff[2], M. Gerin[3], M. De Luca[3], D. A. Neufeld[4], B. Godard[5], and T. G. Phillips[1]
[1] California Institute of Technology, MC 301–17, 1200 E. California Blvd., Pasadena, CA 91125-4700, USA; raquel@caltech.edu
[2] Observatoire de Paris-Meudon, LUTH UMR 8102, 5 Pl. Jules Janssen, F-92195 Meudon Cedex, France
[3] LERMA, CNRS, Observatoire de Paris and ENS, F-75231 Paris Cedex, France
[4] Department of Physics and Astronomy, Johns Hopkins University, 3400 North Charles Street, Baltimore, MD 21218, USA
[5] Departamento de Astrofísica, Centro de Astrobiología (CAB), INTA-CSIC, Crta. Torrejón km 4, E-28850 Torrejón de Ardoz, Madrid, Spain
Received 2012 July 20; accepted 2013 February 26; published 2013 March 26

ABSTRACT

We report the detection of hydrogen chloride, HCl, in diffuse molecular clouds on the line of sight toward the star-forming region W31C (G10.6-0.4). The $J = 1$–0 lines of the two stable HCl isotopologues, $H^{35}Cl$ and $H^{37}Cl$, are observed using the 1b receiver of the Heterodyne Instrument for the Far-Infrared (HIFI) on board the *Herschel Space Observatory*. The HCl line is detected in absorption, over a wide range of velocities associated with diffuse clouds along the line of sight to W31C. The analysis of the absorption strength yields a total HCl column density of a few 10^{13} cm^{-2}, implying that HCl accounts for ∼0.6% of the total gas-phase chlorine, which exceeds the theoretical model predictions by a factor of ∼6. This result is comparable to those obtained from the chemically related species H_2Cl^+ and HCl^+, for which large column densities have also been reported on the same line of sight. The source of discrepancy between models and observations is still unknown; however, the detection of these Cl-bearing molecules provides key constraints for the chlorine chemistry in the diffuse gas.

Key words: astrochemistry – ISM: abundances – ISM: molecules – submillimeter: ISM

Online-only material: color figures

1. INTRODUCTION

Hydride molecules play an important role in interstellar chemistry, as they are often stable end points of chemical reactions, or represent important intermediate stages of the reaction chains theorized to form gas-phase molecules. This makes hydrides a sensitive test of these chemical models, as well as potential tracers of other molecules of interest e.g., molecular hydrogen. Due to their small moment of inertia, hydrides have their fundamental rotational lines in the submillimeter band. The Heterodyne Instrument for the Far-Infrared (HIFI) on board the *Herschel Space Observatory* (Pilbratt et al. 2010) is providing invaluable data on interstellar chemistry in general, and in particular on hydride molecules within the Milky Way and local galaxies. Halogen atoms fluorine (F) and chlorine (Cl), with estimated solar abundances of 3.6×10^{-8} and 3.2×10^{-7} relative to hydrogen (Asplund et al. 2009), are of special interest because they are the major atoms (neutral F and ionic Cl^+) in diffuse environments that react exothermically with molecular hydrogen to form hydride molecules (HF and HCl). HF and HCl are strongly bound systems, only destroyed by photodissociation, reactions with He^+, H_3^+, and C^+ and, in the case of HCl, also by photoionization. Chlorine chemistry has been determined by extensive theoretical and observational work (Jura 1974; Dalgarno et al. 1974; van Dishoeck & Black 1986; Blake et al. 1986; Schilke et al. 1995; Federman et al. 1995). In diffuse clouds, Cl atoms can be ionized by UV photons at wavelengths between 91.2 and 95.6 nm (Jura 1974). The resulting ion, Cl^+, rapidly reacts exothermically (by 0.17 eV) with H_2 to form HCl^+:

$$Cl^+ + H_2 \rightarrow HCl^+ + H, \quad (1)$$

which in turn reacts with H_2 to form chloronium, H_2Cl^+:

$$HCl^+ + H_2 \rightarrow H_2Cl^+ + H. \quad (2)$$

HCl is then formed through dissociative recombination (DR) of H_2Cl^+:

$$H_2Cl^+ + e \rightarrow \begin{cases} Cl + H_2 \\ HCl + H. \end{cases} \quad (3)$$

From reactions (1)–(3), HCl is expected to be abundant in regions containing both H_2 and chlorine-ionizing photons.

Observations of HCl have been limited to ground-based observatories at high-altitude sites, under extreme good weather conditions, or space missions (due to its large rotational constant which places the ground state transition, at 625.9187 GHz, near a strong atmospheric water absorption line). The first detections of interstellar chlorine-containing molecules were obtained using the NASA's Kuiper Airborne Observatory (KAO). Blake et al. (1985) observed the HCl ground-state $J = 1$–0 rotational transition in emission in OMC-1 with angular resolution of about 2′. Zmuidzinas et al. (1995) detected the line in absorption toward Sagittarius B2. Following these results, ground-based observations have led to the detection of the $H^{35}Cl$ and $H^{37}Cl$ isotopologues, in environments such as evolved stars and active star-forming regions (Schilke et al. 1995; Salez et al. 1996; Peng et al. 2010).

Cl chemistry in diffuse clouds on the other hand, has not been fully constrained because of the paucity of observations of Cl-bearing species in the interstellar medium. Prior to *Herschel*/HIFI, HCl in diffuse clouds was observed mainly by means of ultraviolet absorption studies leading only to a tentative detection toward ζ Oph (Federman et al. 1995), with an HCl column density of 2.7×10^{11} cm^{-2}. Given an atomic chlorine column density of 3.0×10^{14} cm^{-2} for this line of sight (Federman et al. 1995), the $N(HCl)/N(Cl)$ ratio is 9×10^{-4}. This result is in good agreement with the theoretical models of the Cl chemistry (van Dishoeck & Black 1986 and more recently Neufeld & Wolfire 2009, hereafter NW09). The NW09 models predict column densities in the range of 10^{10}–10^{12} cm^{-2} for

HCl, H_2Cl^+, and HCl^+, for a diffuse molecular cloud of density $n_H = 10^{2.5}$ cm^{-3} and χ_{UV} in the range of 1–10, where χ_{UV} is the UV radiation field normalized with respect to the mean interstellar value (Draine 1978; see Figures 6 and 7 in NW09). Model predictions also identified H_2Cl^+ and HCl^+ as potentially detectable Cl-bearing species.

The *Herschel*/HIFI instrument has indeed allowed observations for the first time of these two new Cl-bearing species in the interstellar medium, as well as the detection of HCl in diffuse clouds (Lis et al. 2010; De Luca et al. 2012) and in protostellar shocks (Codella et al. 2012). The molecular ions H_2Cl^+ and HCl^+ have been detected in diffuse clouds on the lines of sight to bright submillimeter continuum sources. H_2Cl^+ has been detected in absorption toward NGC 6334I, Sagittarius B2 (S) (Lis et al. 2010), W31C, and Sgr A, and in emission toward Orion Bar and Orion South (Neufeld et al. 2012). The H_2Cl^+ column densities obtained from these studies imply that chloronium accounts for ∼4%–12% of chlorine nuclei in the gas phase. This result is at least a factor of ∼10 larger than that predicted by the chemical models, which predict a H_2Cl^+ and HCl^+ joint contribution of ∼2% to the total gas-phase chlorine budget (Neufeld et al. 2012). Similar results have been derived from observations of HCl^+ toward W31C and W49N (De Luca et al. 2012), where HCl^+ has been detected in absorption with large column densities suggesting a 3%–5% contribution of this species to the total gas-phase chlorine content.

The discrepancy between the chlorine chemistry models and observations is very puzzling; diffuse clouds contain only simple molecules, and the number of reactions involved in describing their abundances is fewer than in dense molecular clouds. Therefore, a test of the basic interstellar chemistry should be possible, establishing much higher standards for the modeling of diffuse clouds compared to those of dense clouds. The diffuse cloud models thus should be able to reproduce the measured abundances to a factor of two or better (van Dishoeck 1990).

In this paper, we report the result of *Herschel*/HIFI observations of HCl $J = 1$–0 on the line of sight toward W31C (G10.6-0.4). These observations were previously attempted by Peng et al. (2010) using the Caltech Submillimeter Observatory (CSO), but yielded no HCl detection due to the high rms of ∼0.15 K at a velocity resolution of 0.31 km s^{-1} in their observations. W31C is an extremely active region of high-mass star formation, and one of the three bright H II regions of the W31 complex, harboring an extremely luminous submillimeter and infrared continuum source ($L_{IR} \sim 10^7\ L_\odot$; Wright et al. 1977). With a kinematic distance of $4.8^{+0.4}_{-0.8}$ kpc (Fish et al. 2003), the W31C line of sight intersects several foreground molecular clouds from the Milky Way spiral arms. The source location and its strong continuum flux make W31C one of the best sources toward which to carry out absorption line studies. We compare the *Herschel*/HIFI results with current chlorine chemistry models and with observations of other Cl-bearing molecules detected along the same line of sight and toward the galactic center source Sgr B2(S).

2. OBSERVATIONS

The observations were performed with the *Herschel*/HIFI instrument (de Graauw et al. 2010) on 2010 March 2, as part of the PRISMAS (Probing Interstellar Molecules with Absorption lines Studies) guaranteed time key program. Both $H^{35}Cl$ and $H^{37}Cl$ $J = 1$–0 lines, with rest frequencies of 625.918 and 624.977 GHz respectively, were observed simultaneously using the HIFI band 1b receiver, with three shifted local oscillator (LO) settings and the wide band spectrometer (WBS). The WBS provides a spectral resolution of 1.1 MHz over a 4 GHz intermediate frequency (IF) bandwidth. The dual beam switch (DBS) observing mode was used with reference beams located 3′ on either side of the source position ($\alpha_{J2000} = 18^h10^m28\overset{s}{.}700$ and $\delta_{J2000} = -19°55'50\overset{''}{.}00$) along an east–west axis.

The data have been reduced using the Herschel Interactive Processing Environment (HIPE; Ott et al. 2010) with pipeline version 5.2. The resulting Level 2 double sideband spectra were exported into FITS format for subsequent data reduction and analysis using the IRAM GILDAS package.[6] The spectra obtained at different LO settings and for each polarization were inspected for possible contamination by emission lines from the image sideband and averaged to produce the final spectra shown in Figure 1. Beam measurements, reported on 2010 November 17, toward Mars at 610 GHz give a main beam (η_{mb}) of 0.744 and 0.764, for the Horizontal (H) and vertical (V) polarization, respectively. The full width at half-maximum (FWHM) HIFI beam size at the HCl $J = 1$–0 frequency is ∼33″.

3. RESULTS

The spectra obtained for the two stable hydrogen chloride isotopologues, $H^{35}Cl$ and $H^{37}Cl$, toward W31C are shown in Figure 1, in the upper and lower panels, respectively. The data quality is excellent with a double sideband continuum antenna temperature of ∼1.6 K, and an rms noise of ∼6 mK. Figure 1 shows the $H^{35}Cl$ and $H^{37}Cl$ emission lines from the background source and a clear absorption feature in the $H^{35}Cl$ spectrum, at velocities ∼10–50 km s^{-1}. The emission lines from the source will be discussed in an extended paper, which will include the HCl observations toward all PRISMAS sources (R. R. Monje et al., in preparation). The $H^{35}Cl$ absorption feature is analogous to the one seen in the spectra of other molecules such as HF, CH, and H_2O (see Figure 2 in Neufeld et al. 2012) and corresponds to the foreground clouds on the line of sight toward W31C. The foreground clouds are known to harbor low density and cool molecular gas ($T_{kin} \sim$ 50–70 K from H_2 and ∼100 K from H I), where molecular excitation can be highly subthermal, with excitation temperatures close to the cosmic microwave background radiation ∼2.73 K (Godard et al. 2010). Consequently, molecular emission lines are very weak and these clouds are best studied through absorption spectroscopy.

The corresponding $H^{37}Cl$ absorption line is contaminated by interfering emission of dimethyl ether (CH_3OCH_3), methyl cyanide (CH_3CN, $v = 0$), and sulfur dioxide (SO_2). The emission lines are modeled with the program XCLASS (Schilke et al. 1998; Comito et al. 2005), which assumes local thermodynamic equilibrium (LTE) and uses the rest frequencies provided by the Cologne Database for Molecular Spectroscopy (CDMS; Müller et al. 2001, 2005) and the Jet Propulsion Laboratory (JPL) molecular spectroscopy database (Pickett et al. 1998). The result from the line fits exhibits two relatively strong CH_3CN and CH_3OCH_3 lines and a weak SO_2 line within the $H^{37}Cl$ absorption spectrum; see Figure 2. To obtain the best LTE fit for CH_3OCH_3 and SO_2, additional lines within the same LO tuning are used; see Figure 2. For CH_3CN, additional transition lines at 533.123 GHz ($J = 29$–28) and 606.533 GHz ($J = 33$–32) are used; see Figure 3. The parameters used in the LTE model, shown in Table 1, assume that CH_3CN and SO_2 are tracers of the hot core (Beltrán et al. 2011) while CH_3OCH_3 arises from the more extended envelope. However, the W31C

[6] http://iram.fr/IRAMFR/GILDAS/

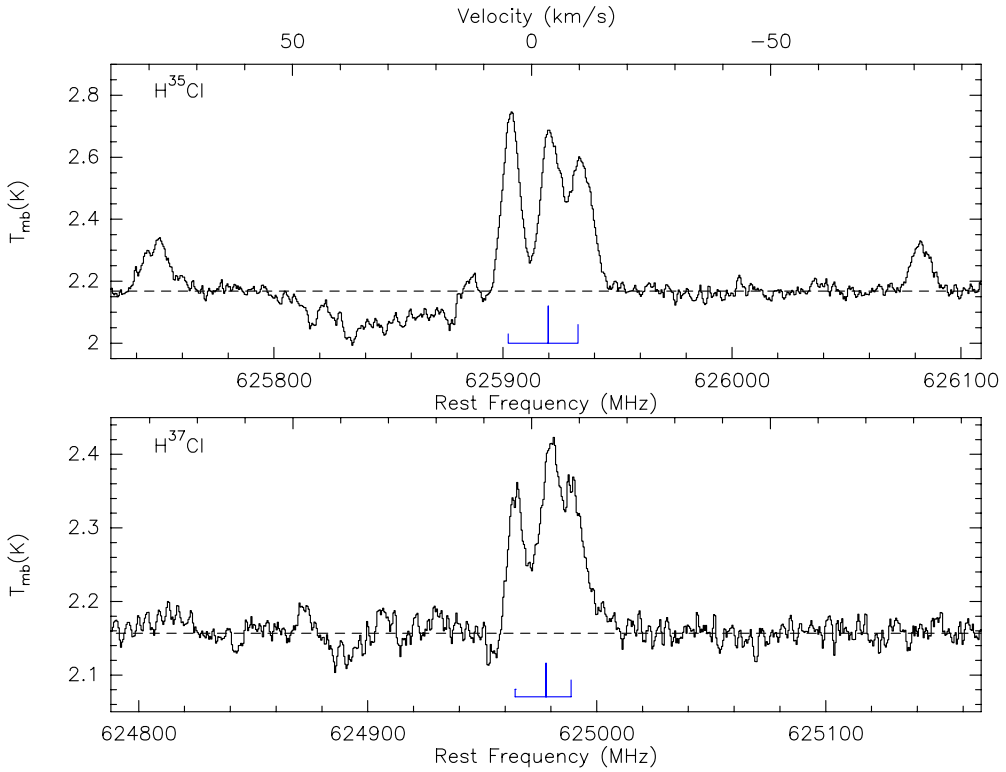

Figure 1. Spectra of the $J = 1$–0 transition of $H^{35}Cl$ (upper panel) and $H^{37}Cl$ (lower panel) toward W31C. The velocity scale in the upper axis is with respect to the frequency of the main ($F = 5/2$–$3/2$) hyperfine component of both isotopologues. The blue lines indicate the position of the HFS components.
(A color version of this figure is available in the online journal.)

Table 1
LTE Model Parameters

Species	Source Size ($''$)	T_{ex} (K)	υ_{LSR} (km s^{-1})	FWHM (km s^{-1})	N (cm^{-2})
CH_3OCH_3	33	60	−2.5	5.5	2×10^{14}
CH_3CN	4	150	−1	5.5	7.4×10^{14}
SO_2	4	150	−1	5	6.5×10^{15}

region is known to be a complex source with outflow activity from embedded high-mass protostars, methanol masers, a dense rotating toroid, and infalling material from the molecular envelope. The LTE emission line fit model is thus an approximation and tighter constraints using the combination of key molecules such as methanol, formaldehyde, CO, CS, and SO, and more complex chemical modeling are needed. Due to the uncertainties of the modeling, we only use the contamination-free spectra (gray shaded area in Figure 2) to derive an estimate of the $^{35}Cl/^{37}Cl$ isotopic ratio, as described below.

The rotational levels of HCl have a hyperfine splitting, caused by the interaction of the quadrupole moment of the chlorine nucleus ($I = 3/2$) and the electric field. The $J = 0$–1 transition is thus split into three components with relative strengths of 50%, 16.7%, and 33.3%, and with velocity offsets ($\Delta\upsilon_h$) of 0, −6.3, and +8.2 km s^{-1} for $H^{35}Cl$, and 0, −5, and 6.5 km s^{-1} for $H^{37}Cl$. The $\Delta\upsilon_h$ is larger than the velocity difference between consecutive velocity components, producing overlaps between different velocity components that result in a complex profile. In order to determine the velocity structure of the foreground absorbing gas, we extract the signal associated with each HFS component using the numerical procedure described in Godard et al. (2012). In Figure 4, we present the $H^{35}Cl$ spectrum, with flux normalized with respect to the single sideband continuum ($2T_L/T_C - 1$, where T_L/T_C is the line-to-continuum ratio) in the velocity range from $\upsilon_{LSR} \approx 5$ to 70 km s^{-1}. The decomposition of the 625 GHz line into three hyperfine components, the main $F = 5/2$–$3/2$ and the two satellite $F = 1/2$–$3/2$ and $F = 3/2$–$3/2$ hyperfine components, is also plotted in Figure 4. We add the three hyperfine components, shifting (in velocity) the satellite components accordingly to the main hyperfine component velocity shift, and obtain a hyperfine deconvolved spectrum, equivalent to a splitting-free spectrum, where each HFS component contributes to the optical depth. In order to estimate the line width and the center velocity of each individual velocity component, we fit the spectrum with a set of Gaussian curves (see Figure 5). The five Gaussian components used in our fit were set to give a better correspondence to other molecular transitions observed toward the same background source, such as H_2Cl^+ (Neufeld et al. 2012) and CH (Gerin et al. 2010). For comparison, we also plot in Figure 5 the $H_2{}^{35}Cl^+$ and $H_2{}^{37}Cl^+$ HFS deconvolved absorption profiles from Neufeld et al. (2012) and the H I absorption spectrum (Fish et al. 2003). The $H_2{}^{35}Cl^+$ and $H_2{}^{37}Cl^+$ profiles are in good agreement with that of $H^{35}Cl$ for most velocity intervals, as expected from precursor species of HCl.

3.1. Column Densities

We calculate the hydrogen chloride column densities for the velocity intervals associated with the different Gaussian components. First, we derive optical depths of the HCl lines ($\tau = -\ln[2T_L/T_C - 1]$), assuming that the foreground absorption completely covers the continuum source and that all HCl

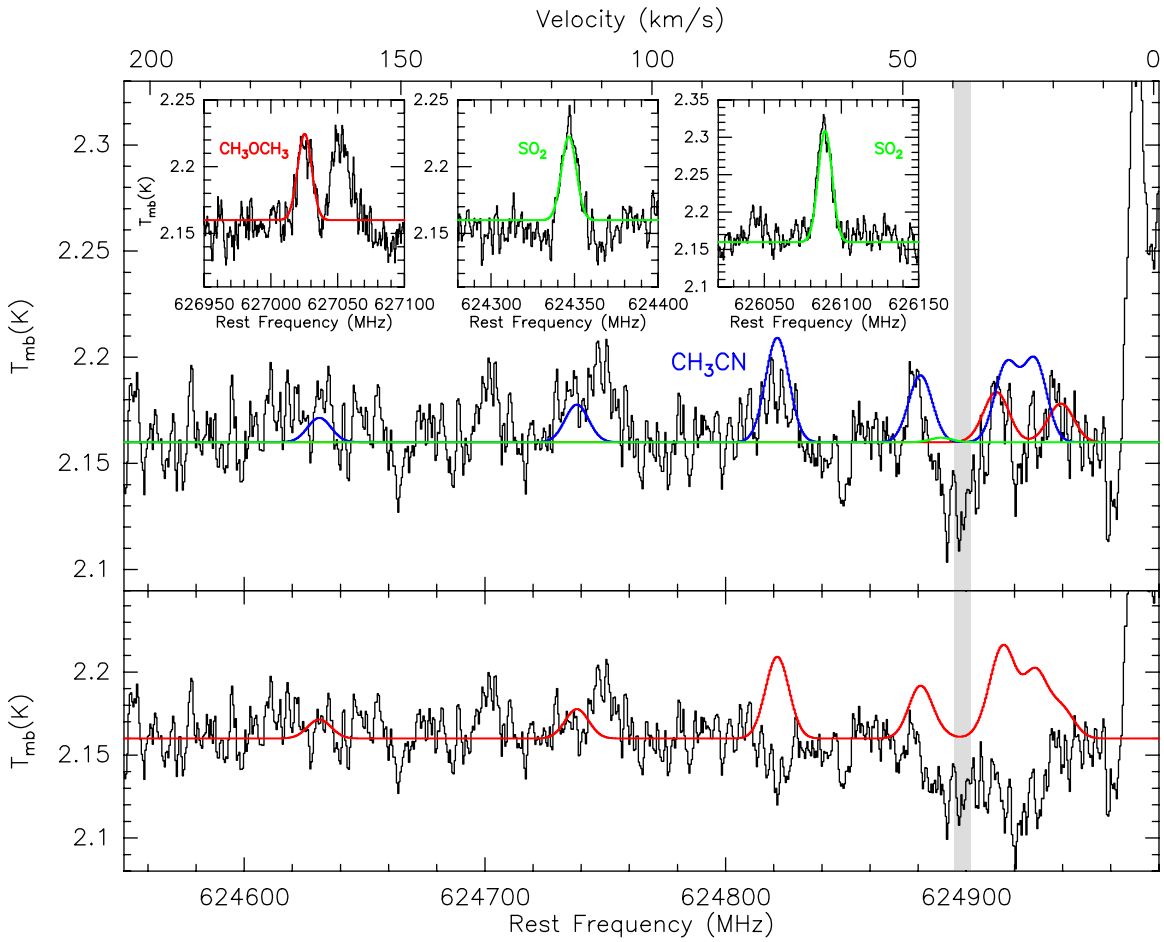

Figure 2. Upper panel: XCLASS LTE models of the dimethyl ether (red), methyl cyanide (blue), and sulfur dioxide (green) emission lines blended into the $H^{37}Cl$ absorption line spectrum, using the parameters given in Table 1. Additional lines (within the observations bandwidth) used in the model are shown in small windows at the top of the plot. The horizontal axis is in frequency units, with the corresponding velocity scale plotted on the top horizontal axis for consistency with Figure 1. Lower panel: for illustration purposes only; shows the resulting $H^{37}Cl$ spectrum (black) after subtracting the contamination from emission lines shown in red. The gray area highlights the emission line contamination-free area within the $H^{37}Cl$ absorption line spectrum.

(A color version of this figure is available in the online journal.)

molecules are in the ground state. We derive the $H^{35}Cl$ column densities for each LSR velocity range using Equation (3) of Neufeld et al. (2010), where the absorption optical depth for the $H^{35}Cl$ $J = 0$–1 transition, integrated over velocity, is given by

$$\int \tau d\upsilon = \frac{A_{ul} g_u \lambda^3}{8\pi g_l} N(\mathrm{H^{35}Cl}) \Rightarrow N(\mathrm{H^{35}Cl}) = 6.5211 \times 10^{12} \int \tau d\upsilon [\mathrm{cm^{-2}}],$$

where $g_u = 3$ and $g_l = 1$ are the degeneracies of the upper ($J = 1$) and lower ($J = 0$) state. Since we use the deconvolved spectrum without hyperfine splitting, $\lambda = 478.96$ μm is the transition wavelength, and $A_{\rm ul} = 1.17 \times 10^{-3}$ $\mathrm{s^{-1}}$ is the spontaneous radiative decay rate. Table 2 shows the HCl column densities and the abundances with respect to the total hydrogen column density. We calculate the $^{35}Cl/^{37}Cl$ ratio in the velocity interval free from emission line contamination (shaded interval in Figure 2), which corresponds to velocities from 38 to 40.5 km $\mathrm{s^{-1}}$. The $^{35}Cl/^{37}Cl$ ratio obtained is equal to 2.9, in good agreement with the solar value of 3.1 (Anders & Grevesse 1989). Thus, the HCl abundances are calculated with respect to the total molecular and neutral hydrogen assuming a $^{35}Cl/^{37}Cl$ of 3.1 in all velocity intervals. The H I column densities in the foreground gas are obtained from Fish et al. (2003), while the molecular hydrogen is obtained from CH (Gerin et al. 2010), assuming a linear correspondence between CH and H_2 with a scaling factor of 3.5×10^{-8} (Sheffer et al. 2008). The average HCl fractional abundance with respect to the total hydrogen is $6.1 \pm 0.6 \times 10^{-10}$. Using a chlorine abundance in diffuse clouds, $N(\mathrm{Cl})/N_{\rm H}$, of 1.03×10^{-7} measured by Moomey et al. (2012) toward nearby (a few hundred parsecs) stars, we obtain that the average fraction of gas-phase Cl in HCl is ∼0.6%.

The uncertainties in the column densities are the random noise and the systematic errors introduced by the calibration uncertainties and the robustness of the HFS decomposition procedure. The 1σ uncertainty in the column density is dominated by the error in the linear baseline fitting. The total HIFI calibration uncertainties for band 1b are $\leqslant$9.3%, which includes the contribution from the sideband gain ratio, beam efficiency, pointing, and hot and cold coupling, where all errors are added in quadrature. Detailed information about the HIFI calibration can be found on Roelfsema et al. (2012). The error introduced by the robustness of the deconvolution procedure is ∼14% (Goddard et al. 2012). Adding in quadrature all the errors, the total uncertainty in the column densities is about 19%.

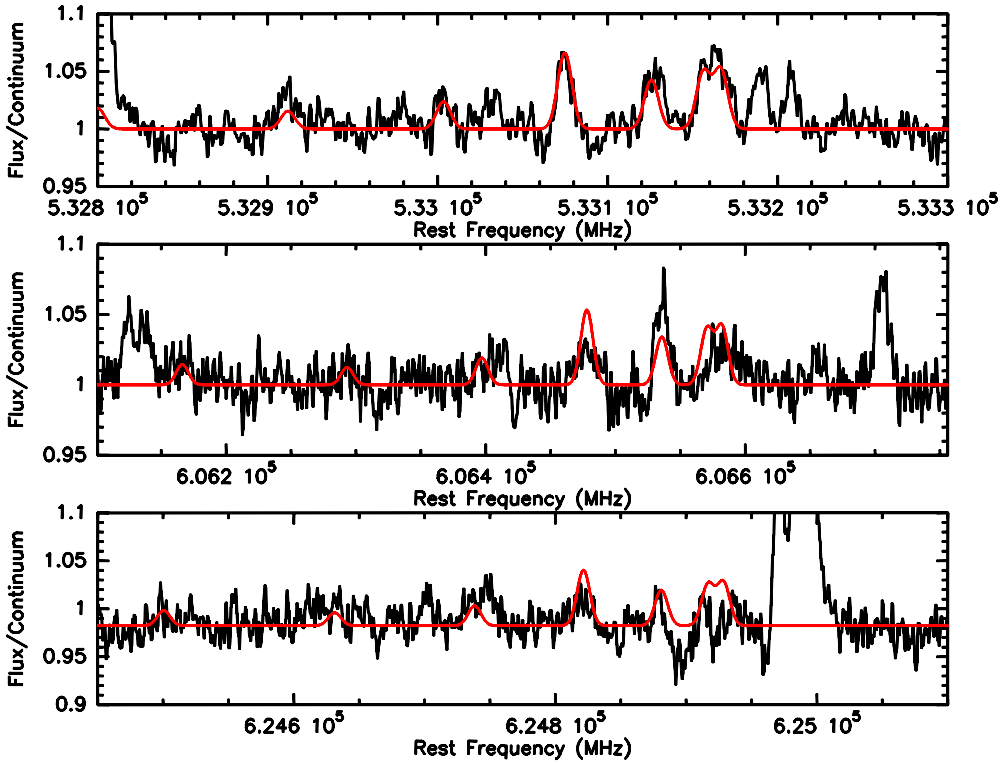

Figure 3. LTE model of CH_3CN (red), using CH_3CN transition lines $J = 29$–28 (upper panel) at 533.123 GHz, $J = 33$–32 (middle panel) at 606.533 GHz, and $J = 34$–33 (lower panel) at 624.878 GHz. The fit parameters are shown in Table 1.

(A color version of this figure is available in the online journal.)

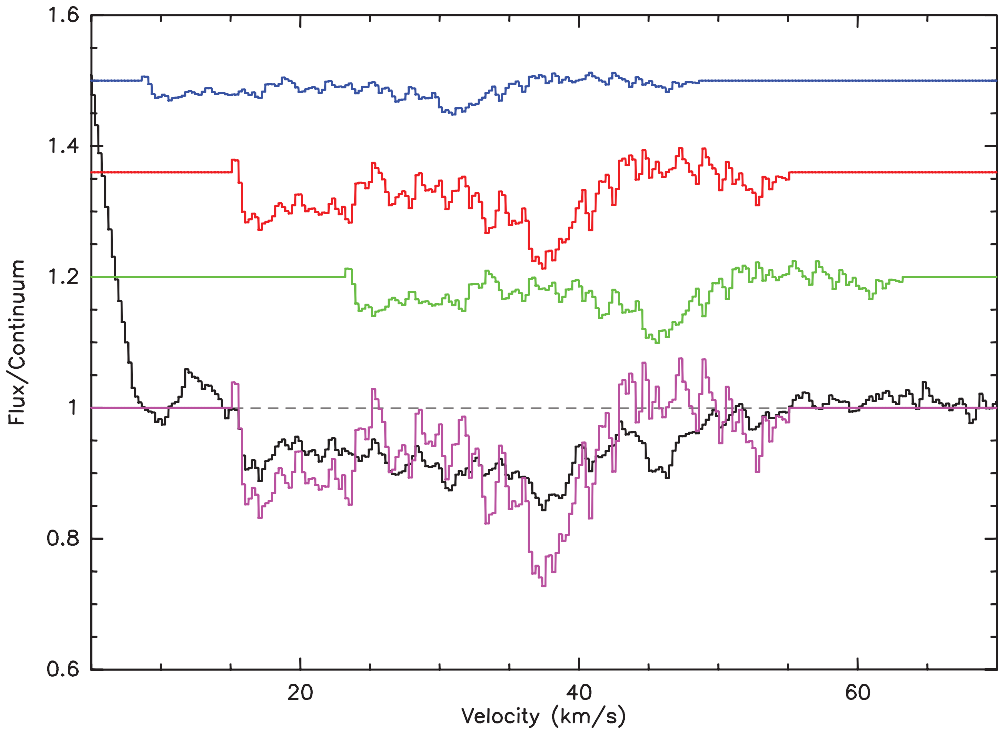

Figure 4. Spectra associated with each HFS component of the $H^{35}Cl$ line: $F_1 = 3/2$–$3/2$, $F = 2$–2 (green), $F_1 = 5/2$–$3/2$, $F = 3$–2 (blue); $F_1 = 1/2$–$3/2$, $F = 1$–2 (red; vertical offset introduced for clarity), the sum of the three components (magenta), and the observed spectrum (black).

(A color version of this figure is available in the online journal.)

Table 2
HCl Column Densities and Abundances on the Line of Sight toward W31C

v_{LSR} (km s^{-1})	N(H I)[a] ($\times 10^{21}$ cm^{-2})	$N(H_2)$[b] ($\times 10^{21}$ cm^{-2})	$N(H^{35}Cl)$ ($\times 10^{12}$ cm^{-2})	N(HCl)[c] ($\times 10^{12}$ cm^{-2})	N(HCl)/N_H[d] ($\times 10^{-10}$)
[15, 19]	1.3 ± 0.35	2.9 ± 0.3	2.8 ± 0.51	3.7 ± 0.67	5.2 ± 1.1
[19, 24]	1.6 ± 0.56	2.7 ± 0.3	3.8 ± 0.69	5.0 ± 0.91	7.1 ± 1.5
[25, 29]	1.6 ± 0.40	3.6 ± 0.3	1.3 ± 0.28	1.7 ± 0.37	1.9 ± 0.5
[30, 36]	2.1 ± 0.78	3.5 ± 0.3	4.0 ± 0.74	5.3 ± 0.98	5.9 ± 1.2
[36, 40]	1.7 ± 0.20	3.0 ± 0.3	6.0 ± 1.02	8.0 ± 1.3	10.3 ± 1.9
[15, 40]	8.4 ± 1.12	15.6 ± 0.7	17.8 ± 1.2	23.6 ± 2.1	6.0 ± 0.6

Notes.
[a] The H I column densities are obtained from Fish et al. (2003) absorption data with $N(\mathrm{H\,I}) = 1.84 \times 10^{20}(T_{spin}/100\ \mathrm{K})\int \tau_{\mathrm{H\,I}} dv$ [cm^{-2}/km s^{-1}], assuming a $T_{spin} \sim 100$ K.
[b] The H_2 column densities are derived from CH observations (Gerin et al. 2010), assuming $N(\mathrm{CH}) = 3.5 \times 10^{-8}\ N(H_2)$ (Sheffer et al. 2008).
[c] Assuming a solar $^{35}Cl/^{37}Cl$ ratio of 3.1.
[d] $N_H = 2N(H_2) + N(\mathrm{H\,I})$.

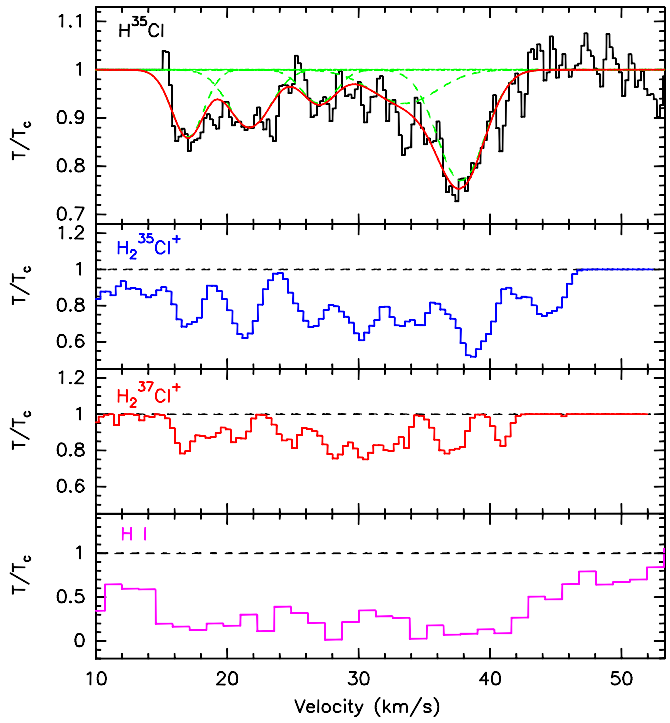

Figure 5. Top panel: multiple Gaussian fits (red) to the hyperfine deconvolved spectrum of $H^{35}Cl$ $J = 0$–1 (black) associated with foreground clouds on the line of sight toward W31C. For comparison, we show the HFS deconvolved spectra of $H_2{}^{35}Cl^+$ (blue), $H_2{}^{37}Cl^+$ (red) from Neufeld et al. (2012), and H I (magenta) from Fish et al. (2003).

(A color version of this figure is available in the online journal.)

4. CHEMICAL MODEL

We use the Meudon PDR code (Le Petit et al. 2006) to compute the fractional abundances of the various chlorine bearing species, i.e., the abundance of each species normalized relative to the chlorine elemental abundance, as a function of the total extinction of the cloud, $A_{v,tot}$. The Meudon PDR code is a one- or two-sided model, where the molecular cloud is modeled as a stationary plane-parallel slab of gas and dust, exposed to incident radiation field from a bright star or the Interstellar Standard Radiation Field (ISRF). As input parameters, we use the best fit model from Neufeld et al. (2012), which corresponds to an initial density of $n_H = 316$ cm^{-3}, a radiation field intensity of 10 from both sides, and a primary ionization rate of 1.810×10^{-16} s^{-1}. Using the standard Galactic gas-to-dust ratio $N_H/A_v = 1.93 \times 10^{21}$ mag^{-1} cm^{-2} (Whittet 2003), $A_{v,tot}$ probed is ∼3–5. The obtained abundances normalized relative to the relevant gas-phase elemental abundance are shown in Figure 6 (left); the results indicate that the HCl^+ and H_2Cl^+ account jointly at best for ∼2% of the elemental chlorine in the gas phase while HCl accounts for ∼0.1%. The modeled HCl fractional abundance underpredicts the results obtained from the observations by an average value of about 6.

The DR studies of H_2Cl^+ and the corresponding product branching ratios are not yet available from laboratory experiments. In their models, NW09 assumed a branching ratio of 90% for Cl and 10% for HCl, motivated by the low HCl abundance observed toward the diffuse cloud ζ Oph. We have thus investigated the effect of the branching ratio of H_2Cl^+ DR for the physical conditions described above, based on the correlation obtained between the branching ratio of triatomic dihydride ions for three-body dissociation and the corresponding energy release obtained by Roueff & Herbst (2011). From that correlation, Roueff & Herbst (2011) obtain a branching ratio of 56% for the three-body dissociation of H_2Cl^+. We estimate the fractional abundances corresponding to the new branching ratio and plot them as dashed lines in Figure 6 (right), in comparison with those obtain with previous assumption (90% for Cl) in full lines, as a function of $A_{v_{tot}}$. The results show that differences occur only for the minor species, i.e., HCl, HCl^+, and H_2Cl^+ while the reservoirs Cl and Cl^+ are not affected. The increase in the HCl column density is about a factor of ∼5, in closer agreement with our observational results. However, the increase for HCl^+ and H_2Cl^+ is much smaller, and so this result cannot explain all the discrepancies.

5. DISCUSSION

We present the detection of $H^{35}Cl$ and $H^{37}Cl$ $J = 0$–1 transition in absorption on the line of sight toward the bright submillimeter source W31C. The obtained HCl column density (∼2×10^{13} cm^{-2}), is comparable with that obtained toward the line of sight to Sgr B2 (S) (Lis et al. 2010). Given the HCl^+ and H_2Cl^+ column densities from De Luca et al. (2012) and Neufeld et al. (2012), the HCl^+/H_2Cl^+ and HCl/H_2Cl^+ column density ratios of ∼1 and ∼0.3, respectively, are within the range predicted by the models of diffuse clouds. However, the averaged HCl abundance with respect to the total hydrogen content of $6.1 \pm 0.6 \times 10^{-10}$ suggests a HCl fractional abundance with respect to the chlorine elemental abundance

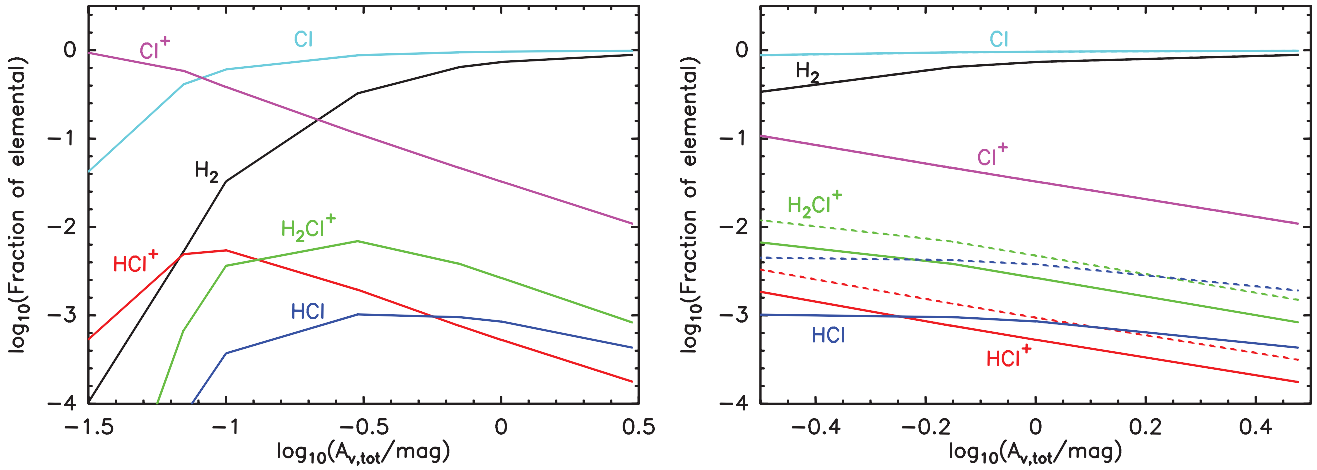

Figure 6. Left: abundance of the Cl-bearing molecules, chlorine atom or ion (X), normalized relative to the gas-phase chlorine abundance, $\overline{f}(\mathrm{X}) = N(\mathrm{X})/N(\mathrm{Cl})$, obtained with the Meudon PDR code, Cl^+ (magenta), Cl (cyan), HCl (blue), HCl^+ (red), and H_2Cl^+ (green) together with the H_2 fractions (black), $\overline{f}(\mathrm{X}) = 2N(\mathrm{H_2})/(2N(\mathrm{H_2}) + N(\mathrm{H\,I}))$, averaged along the line of sight, as a function of total visual extinction $A_{v,\mathrm{tot}}$. The initial density is $n_{\mathrm{H}} = 316\ \mathrm{cm}^{-3}$, and the radiation field intensity is 10. Right: comparison of the predicted fraction of gas-phase chlorine present in HCl, HCl^+, H_2Cl^+, Cl, and Cl^+ assuming a branching ratio of 90% for chlorine and 10% for hydrogen chloride (solid lines) and the predicted fractions for a reduced branching ratio of 56% for chlorine (dashed line).

(A color version of this figure is available in the online journal.)

$(N(\mathrm{Cl})/N_{\mathrm{H}} = 1.03 \times 10^{-7})$, a factor of about 6 larger than those predicted by chemical models of diffuse clouds. Similar discrepancies between models and observations were also found for other Cl-bearing gas-phase species, HCl^+ and H_2Cl^+ toward W31C, Sgr A (+50 km s^{-1} molecular cloud), and W49N (Lis et al. 2010; De Luca et al. 2012; Neufeld et al. 2012).

Lis et al. (2010) suggested a geometrical explanation for the discrepancy between the observed column densities and the models, where enhancement in the absorbing column density could result from multiple PDRs present along the line of sight. This scenario could explain higher column densities, but the HCl/Cl ratio will remain constant and hence this solution is not likely to reproduce the W31C line of sight results.

Neufeld et al. (2012) explored several possible explanations for the deficiencies in the model predictions, e.g., the rate coefficient assumed for dissociative recombination (DR) of HCl^+ and uncertainties in the assumed dipole moment of H_2Cl^+, none of which proved satisfactory. We have investigated the effect of varying the branching ratio of H_2Cl^+ DR. By taking a branching ratio of 56% for the chlorine (instead of 90% assumed in NW09 models), the predicted fractional abundance of HCl with respect to the gas-phase chlorine abundance increases by about a factor of ∼5. However, laboratory results are needed to confirm the branching ratio and validate this argument, along with the study of other unknowns in the chlorine chemistry, such as the DR rates, and the dipole moment of H_2Cl^+.

HIFI has been designed and built by a consortium of institutes and university departments from across Europe, Canada, and the United States (NASA) under the leadership of SRON, Netherlands Institute for Space Research, Groningen, The Netherlands, and with major contributions from Germany, France, and the US. Consortium members are Canada: CSA, U. Waterloo; France: CESR, LAB, LERMA, IRAM; Germany: KOSMA, MPIfR, MPS; Ireland: NUI Maynooth; Italy: ASI, IFSI-INAF, Osservatorio Astrofisico di Arcetri-INAF; The Netherlands: SRON, TUD; Poland: CAMK, CBK; Spain: Observatorio Astronomico Nacional (IGN), Centro de Astrobiologia; Sweden: Chalmers University of Technology - MC2, RSS & GARD, Onsala Space Observatory, Swedish National Space Board, Stockholm University - Stockholm Observatory; Switzerland: ETH Zurich, FHNW; USA: CalTech, JPL, NHSC. Support for this work was provided by the Centre National de Recherche Spatiale (CNES), by the SCHISM project (grant ANR-09-BLAN-0231-01), by NASA through an award issued by JPL/Caltech, and by the Spanish MICINN (grants AYA2009-07304 and CSD2009-00038). This research has been supported in part by the NSF, award AST-0540882 to the CSO.

Facility: Herschel (HIFI)

REFERENCES

Anders, E., & Grevesse, N. 1989, GeCoA, 53, 197
Asplund, M., Grevesse, N., Sauval, A. J., & Scott, P. 2009, ARA&A, 47, 481
Blake, G. A., Anicich, V. G., & Huntress, W. T., Jr. 1986, ApJ, 300, 415
Blake, G. A., Keene, J., & Phillips, T. G. 1985, ApJ, 295, 501
Beltrán, M. T., Cesaroni, R., Neri, R., & Codella, C. 2011, A&A, 525, A151
Codella, C., Ceccarelli, C., Bottinelli, S., et al. 2012, ApJ, 744, 164
Comito, C., Schilke, P., Phillips, T. G., et al. 2005, ApJS, 156, 127
Dalgarno, A., de Jong, T., Oppenheimer, M., & Black, J. H. 1974, ApJL, 192, L37
De Graauw, Th., Helmich, F. P., Phillips, T. G., et al. 2010, A&A, 518, L6
De Luca, M., Gupta, H., Neufeld, D., et al. 2012, ApJL, 751, L37
Draine, B. T. 1978, ApJS, 36, 595
Federman, S. R., Cardelli, J. A., van Dishoeck, E. F., Lambert, D. L., & Black, J. H. 1995, ApJ, 445, 325
Fish, V. L., Reid, M. L., Wilner, D. J., & Churchwell, E. 2003, ApJ, 587, 701
Gerin, M., de Luca, M., Goicoechea, J. R., et al. 2010, A&A, 512, L16
Godard, B., Falgarone, E., Gerin, M., Hily-Blant, P., & De Luca, M. 2010, A&A, 520, 20
Godard, B., Falgarone, E., Gerin, M., et al. 2012, A&A, 540, A87
Jura, M. 1974, ApJL, 190, L33
Le Petit, F., Nehmé, C., Le Bourlot, J., & Roueff, E. 2006, ApJS, 164, 506
Lis, D. C., Pearson, J. C., Neufeld, D. A., et al. 2010, A&A, 521, L9
Moomey, D., Federman, S. R., & Sheffer, Y. 2012, ApJ, 744, 174
Müller, H. S. P., Schlöder, F., Stutzki, J., & Winnewisser, G. 2005, JMoSt, 742, 215
Müller, H. S. P., Thorwirth, S., Roth, D. A., & Winnewisser, G. 2001, A&A, 370, L49
Neufeld, D. A., Roueff, E., Snell, R. L., et al. 2012, ApJ, 748, 37
Neufeld, D. A., Sonnentrucker, P., Phillips, T. G., et al. 2010, A&A, 518, L108
Neufeld, D. A., & Wolfire, M. G. 2009, ApJ, 706, 1584 (NW09)
Ott, S. 2010, in ASP Conf. Ser. 434, Astronomical Data Analysis Software and Systems XIX, ed. Y. Mizuno, K. I. Morita, & M. Ohishi (San Francisco, CA: ASP), 139
Peng, R., Yoshida, H., Chamberlin, R., et al. 2010, ApJ, 723, 218
Pickett, H. M., Poynter, I. R. L., Cohen, E. A., et al. 1998, JQSRT, 60, 883

Pilbratt, G. L., Riedinger, J. R., Passvogel, T., et al. 2010, A&A, 518, L1
Roelfsema, P. R., Helmich, F. P., Teyssier, D., et al. 2012, A&A, 537, A17
Roueff, E., & Herbst, E. 2011, JPhCS, 300, 2028
Salez, M., Frerking, M. A., & Langer, W. D. 1996, ApJ, 467, 708
Schilke, P., Phillips, T. G., & Mehringer, D. M. 1999, in Proc. 3rd Cologne-Zermatt Symposium, The Physics and Chemistry of the Interstellar Medium, ed. V. Ossenkopf, J. Stutzki, & G. Winnewisser (Herdecke: GCA-Verlag), 330
Schilke, P., Phillips, T. G., & Wang, N. 1995, ApJ, 441, 334
Sheffer, Y., Rogers, M., & Federman, S. R. 2008, ApJ, 687, 1075
Sonnentrucker, P., Neufeld, D. A., Phillips, T. G., et al. 2010, A&A, 521, L12
van Dischoeck, E. F. 1990, in ASP Conf. Ser. 12, The Evolution of the Interstellar Medium, ed. L. Blitz (San Francisco, CA: ASP), 207
van Dischoeck, E. F., & Black, J. H. 1986, ApJS, 62, 109
Whittet, D. 2003, Lunar Planet. Inf. Bull., 94, 11
Wright, E. L., Fazio, G. G., & Low, F. J. 1977, ApJ, 217, 724
Zmuidzinas, J., Blake, G. A., Carlstrom, J., Kneene, J., & Miller, D. 1995, ApJL, 447, L125